Electrochemistry Communications 136 (2022) 107242

Contents lists available at ScienceDirect

Electrochemistry Communications

journal homepage: www.elsevier.com/locate/elecom

Methylated DNA impedimetric immunosensor based on azo-polymer-AuNPs dots and 5-methylcytosine antibody using dissolved oxygen as a redox probe

André Olean-Oliveira [a], Patricia Monteiro Seraphim [b], Marcos F.S. Teixeira [a,*]

[a] Department of Chemistry and Biochemistry – School of Science and Technology, Sao Paulo State University (UNESP), Rua Roberto Simonsen, 305, CEP 19060-900 – Presidente Prudente, SP, Brazil

[b] Department of Physiotherapy – School of Science and Technology, Sao Paulo State University (UNESP), Rua Roberto Simonsen, 305, CEP 19060-900 - Presidente Prudente, SP, Brazil

ARTICLE INFO

Keywords:
Methylated DNA sensor
Immunosensor
Gold nanoparticle-polymer
Methylcytosine antibody
Secondary antibody less

ABSTRACT

The present work describes the development of an electrochemical immunosensor for the direct determination of methylated DNA using dissolved oxygen as the redox probe. The oxygen-sensitive response is possible due to the presence of a redox conducting polymer based on the Bismarck Brown Y dye (poly(azo-BBY)). In addition to the azo-polymer, gold nanoparticles (AuNPs) were formed in the polymer film by encapsulation to increase the active surface area and enhance sensor performance. The platform was easily synthesized using a single-step electropolymerization technique in a solution containing the BBY monomer and $HAuCl_4$ salt. The immunosensor was developed by simply immobilizing the 5-methylcytosine antibody (Ab-5-mC) with high affinity to 5-mC on the surface of a device coated with azo-polymer-AuNPs dots. No secondary antibodies or enzymes were used in constructing this device. The immunosensor performance was evaluated by electrochemical impedance spectroscopy (EIS) in different concentrations of 5-methylcytosine (5-mC) in 0.10 mol L^{-1} phosphate buffer solution (PBS) solution containing atmospheric oxygen. A calibration curve was obtained by varying the resistance of the system as a function of the 5-mC concentration, revealing a limit of detection (LOD) in picograms per milliliter.

1. Introduction

Scientific studies determining biomarkers for specific diseases have profound implications for the advancement of health and clinical practice [1–3]. In this sense, electrochemical immunosensors have shown notable prominence due to the possibility of minimizing the cost of immunological analysis by reducing the time and number of steps involved [4,5]. Furthermore, electrochemical systems can be easily miniaturized and are widely targeted for use as transducers in point-of-care (PoC) devices [6,7]. Immunosensors based on electrochemical impedance spectroscopy (EIS) stand out as a transduction model, mainly due to the high sensitivity achieved by the technique, which can reach detection limits at the picomole scale [8–10]. Most of these works use ferrocene as a redox species in solution to increase the signal-to-noise (S/N) response to antigen–antibody interactions at the electrode surface. However, the presence of excess redox probes can be accompanied by problems associated with false-positive sensor responses [11,12]. This study proposes an alternative methodology using dissolved oxygen, already naturally present in the reaction system, as a redox probe for the detection of 5-methylcytosine for the determination of global levels of methylated DNA. The immunosensor was developed by the direct response of the 5-methylcytosine antibody immobilized on the device surface, without the need for a secondary antibody or enzyme. To the best of our knowledge, this is the first work in the literature to propose this methodology. This approach is possible due to the selective and sensitive response to the dissolved oxygen reduction reaction of the redox conducting polymer Bismarck Brown Y [13–16]. Furthermore, gold nanoparticles (AuNPs) were generated in situ from the polymer which tended to increase the active surface area and improve the performance of the nanocomposite in the dot structure [17].

* Corresponding author.
E-mail address: marcos.fs.teixeira@unesp.br (M.F.S. Teixeira).

https://doi.org/10.1016/j.elecom.2022.107242
Received 17 January 2022; Received in revised form 3 February 2022; Accepted 7 February 2022
Available online 10 February 2022

2. Materials and methods

All measurements were performed using a three-electrode configuration: a saturated calomel electrode (SCE) for the electropolymerization step and pseudo-Ag/AgCl for aqueous solution measurements as the reference electrode, platinum wire as the counter electrode and a fluorine-doped tin oxide (FTO) electrode coated with poly(azo-BBY)-AuNPs as the working electrode. The electrochemical measurements were performed with a PalmSens3 interfaced with PSTrace 5.8 software. All reagents used were of high purity ≥ 98% (Sigma Aldrich).

The poly(azo-BBY)-AuNP nanomaterial on the FTO surface was prepared by a single-step technique [16] by potential cycling between −0.30 and + 1.00 V (vs. SCE) for 20-cycle scans at a scan rate of 10 mV s^{-1} in a deaerated solution containing 10 mmol L^{-1} BBY monomer and 1.00 mmol L^{-1} $HAuCl_4$ in 0.10 mol L^{-1} HCl medium. Then, the films were rinsed with deionized water and stored in a plastic container at room temperature. The immunosensor preparation was carried out by covalent immobilization of 5-methylcytosine antibody (Ab-5-mC) using glutaraldehyde (Glu) on the azo-polymer-AuNPs dots. In summary, before immobilizing the antibody on the surface of the device coated with poly(azo-BBY)-AuNPs, the surface was rinsed with a 0.10 mol L^{-1}

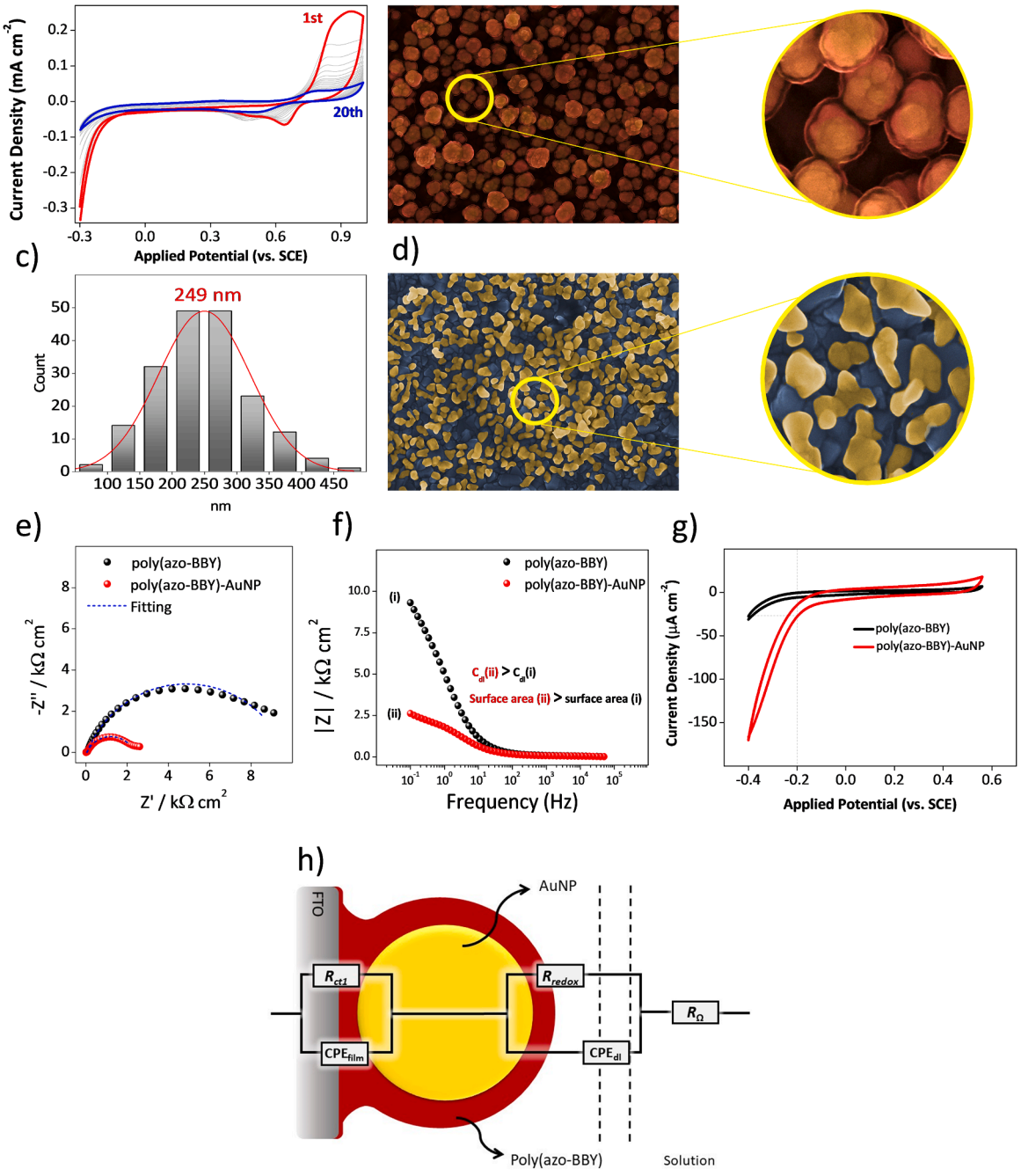

Fig. 1. Electrosynthesis and characterization of the nanocomposite. (a) Cyclic voltammogram for poly(azo-BBY)-AuNP electropolymerization on an FTO electrode. (b) and (d) SEM images (100.0 k × magnification) of the nanocomposite FTO/poly(azo-BBY)-AuNP film and FTO/AuNPs, respectively. (c) Histogram of the poly(azo-BBY)-AuNP nanoparticle size distribution. (e) EIS applying a DC potential of −0.20 V (vs. SCE) for poly(azo-BBY) and poly(azo-BBY)-AuNPs in 0.05 mol L^{-1} PBS solution in an O_2 atm. (f) Bode diagram corresponding to the EIS measurements. (g) Electrochemical characterization of poly(azo-BBY) and poly(azo-BBY)-AuNPs in 0.05 mol L^{-1} PBS solution under O_2 saturation using cyclic voltammetry at 25 mV s^{-1}. (h) Electrical circuit model for mathematical spectra adjustment.

PBS solution (pH 7.40). After washing with buffer, 20 μL of 5% ($^{m}/_{v}$) glutaraldehyde solution was dropped on the surface and left for 5 min. Excess glutaraldehyde on the device surface was removed by successive rinsing with buffer solution. Subsequently, 20.0 μL of 1.0 μg mL^{-1} 5-methylcytosine antibody (Ab-5-mC) solution was added and allowed to incubate at room temperature for 30 min. Again, the poly(azo-BBY)-AuNP/Ab-5-mC-coated device was gently washed with buffer. The glutaraldehyde active sites remaining on the polymer surface were deactivated by incubating with a 1% bovine serum albumin (BSA) solution for 30 min. Finally, the immunosensor was washed and used for impedimetric measurements. When not in use, the immunosensor was stored in a refrigerator in a PBS solution at −4 °C. The EIS measurements were performed by applying the incidence of a 10-mV sine wave with a frequency range of 50 kHz to 0.1 Hz with 10 step/dec. All spectra were recorded at 25 °C. The complex plane impedance spectra were analyzed using EIS Analyzer 1.0 software. To fit the complex plane impedance spectra using the software, the capacitive element was replaced by a constant phase element (CPE). This is a nonideal capacitor with CPE = $1/Q(j\omega)^{\alpha}$, where α is an exponent with values between 0 and 1. The real (C') and imaginary (C'') capacitance values were obtained from $C'(\omega) = Z''/\omega Z^2$ and $C''(\omega) = Z'/\omega Z^2$, where ω is the angular frequency [12]. The immunoassay was carried out by exposing the sensor to different concentrations of 5-methylatedcytosin (5-mC) in PBS solution for 40 min and performing EIS measurements. The R_{redox} values obtained by the equivalent circuit model were normalized as follows:

$$R_{relative}(\%) = \frac{R_{redox} - R_0}{R_0} \times 100 \quad (1)$$

where R_0 is the resistance in the absence of 5-mC.

3. Results

3.1. In situ single-step encapsulation of gold nanoparticles by the redox polymer and its impedimetric response to dissolved oxygen

The poly(azo-BBY)-AuNP nanocomposite film was synthesized by cyclic voltammetry, applying 20 potential cycles over an interval of −0.30 to + 1.0 V (vs. SCE) at a scan rate of 10 mV s^{-1} (Fig. 1a). Fig. 1a shows that during the cycle scans, the current assigned to the cation radical decreases (potential between 0.80 and 0.90 V) due to the coverage of the FTO surface by the nanocomposite. On the other hand, the current related to the redox polymer response progressively increased (0.0–0.50 V) [16,18]. The polymer dots obtained after the 20th applied potential cycle were characterized by scanning electron microscopy (SEM) (Fig. 1b). The SEM image shows the formation of gold nanoparticles in the form of nanoclusters encapsulated by a thin layer of poly(azo-BBY) evenly distributed over the entire surface of the device. Furthermore, imaging showed that the nanostructures varied in dimension between 74 and 475 nm, with an average value of 249 nm (Fig. 1c). The same structures are not observed on the conductive substrate when using a solution containing only tetrachloroauric(III) acid (Fig. 1d). In fact, the absence of stabilizer molecules (such as polymers) makes it infeasible to use nanoparticles due to their instability, as they do not present a regular and well-defined shape due to the dissolution and redeposition processes caused by cyclic voltammetry [17,19].

Fig. 1(e) and (f) show typical electrochemical impedance data for poly(azo-BBY)-AuNP and poly(azo-BBY) films. The spectra obtained were analyzed using an equivalent circuit model (Fig. 1h) for the mathematical determination of the impedimetric parameters. The equivalent circuit proposed for the present device represents two interfacial resistance phenomena related to charge transfer at the poly (azo-BBY)–AuNP (R_{ct1}) interface and the reduction reaction of dissolved O_2 by the azo group in the polymer layer (R_{redox}) that covers the gold nanoparticles (Eq. (2)). The R_{ct} values are accompanied in parallel by the polymer film (CPE_{film}) and double layer (CPE_{dl}) capacitances. EIS measurements performed in PBS solution with saturated dissolved oxygen (40 mg mL^{-1} O_2) show that an increase in the electrochemical active surface area for the polymer-AuNP-coated device can be observed. This typical behavior is examined by the decrease in the impedimetric response slope in the range of low to medium frequencies in the Bode spectrum (Fig. 1f). The electrochemically active surface areas of the devices were calculated from the redox capacitance values [20,21]. The electroactive area of the poly(azo-BBY)-AuNP nanocomposite-coated device was 62% higher than that of the device coated with only the polymer. This significant increase results in an increase in active nitrogen group sites from the molecular structure of the poly(azo-BBY) (highlighted in red in Fig. 2c) for antibody immobilization in immunosensor construction. In addition, the redox (azo moieties) sites of the polymer are more available for reaction with dissolved oxygen (Eq. (2)), resulting in increased sensitivity of the device. By analyzing the voltammetric response (see Fig. 1g), it is possible to observe a decrease in the electroreduction overpotential of the oxygen, followed by a significant increase in the cathodic current of the system.

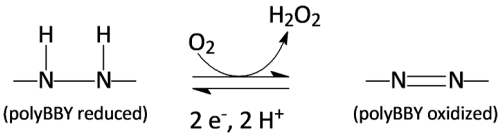

(2)

Aanalysis of the element impedimetric parameters (Table S1) revealed that the presence of dissolved oxygen decreased the R_{redox} value, as observed in previous studies. This wide sensitivity of the poly (azo-BBY)-AuNP-coated device to the variation of oxygen in solution will be used as a redox probe to accompany the analysis of methylated DNA.

3.2. Construction of the immunosensor and its impedimetric behavior

Fig. 2(a-b) illustrates the EIS data for each step of device modification in immunosensor composition. Glutaraldehyde was used as a linker to covalently bind the antibody to the sensor surface [12,22]. In turn, BSA was applied after immunosensor construction to block the free glutaraldehyde on the polymer and prevent direct access of the analyte to the redox site, preventing false-positive results in the analytical signal [23,24]. Table 1 presents the impedimetric parameters obtained for each type of prepared device. Evidence of the modifications applied to the surface of the nanocomposite is observed by an increase in the capacitive arc (see Fig. 2a), indicating a decrease in molecular oxygen access to the polymer redox site. Looking at the R_{redox} parameter in Table 1, there is an increase in charge transfer resistance from 22.4 to 112 kΩ cm^2, corresponding to the device covered with nanocomposite (Fig. 2c1) and the device after all the modification steps (Fig. 2c4). Despite the significant increase in the R_{redox} value, impedimetric measurements (Fig. S1) with the complete device in solutions containing 0.0 and 99.1% dissolved O_2 showed that the sensor retained direct sensitivity to dissolved oxygen.

A good method of studying possible biomolecular surface alterations is through complex capacitance analysis of impedance data [11]. The surface modifications also resulted in the alteration of the redox capacitance (C_{redox}), as illustrated in Fig. 2B. This 68% decrease in redox capacitance represents a high degree of surface modification when anchoring the Ab-5-mC antibody.

3.3. Immunosensor evaluation from methylated cytosine

There are several common ways of determining whether a gene contains methylated DNA [25–28]. The most commonly used protocol is the treatment of DNA with bisulfite and the quantification of the methylation status using methylated cytosine standards. The impedance response of the poly(azo-BBY)-rGO film to different concentrations of methylated cytosine was carried out in a PBS (pH 7.4) solution

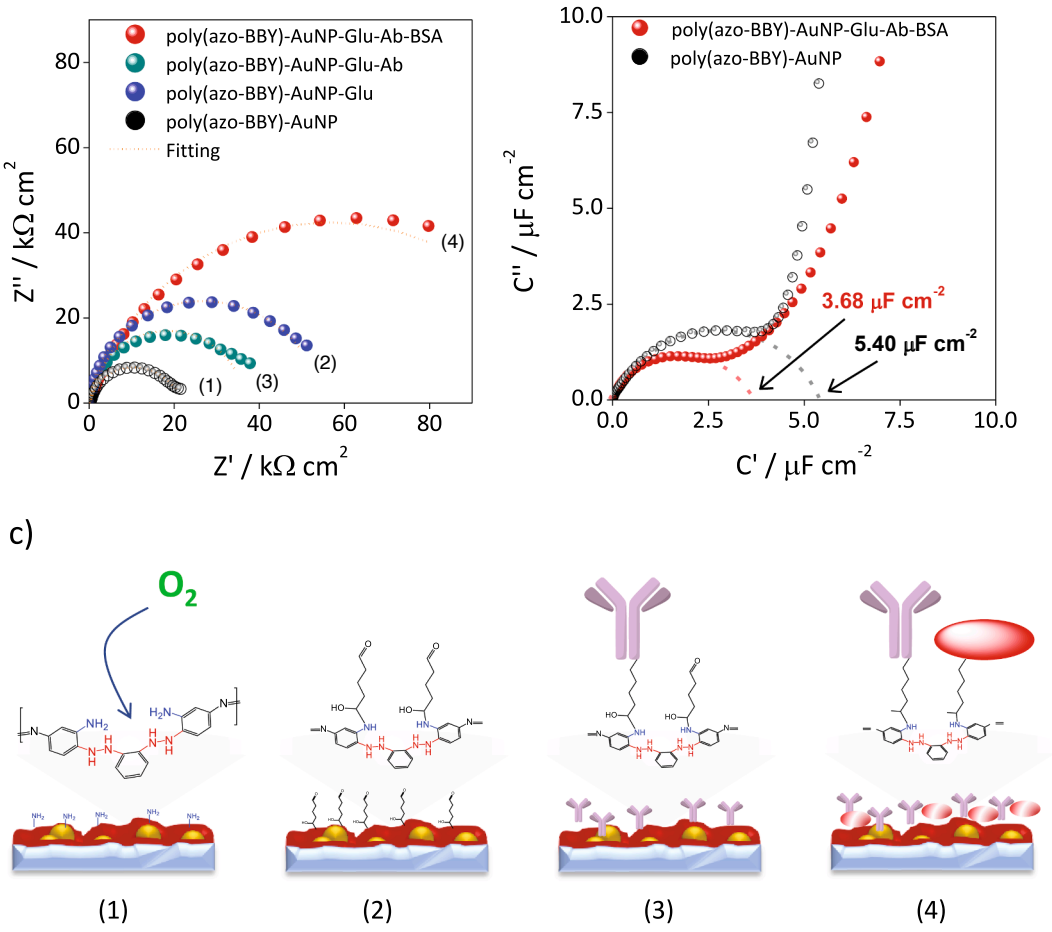

Fig. 2. Impedimetric characterization of the 5-mC immunosensor. (a) Nyquist spectra for each modification step with an applied potential of −0.40 V (vs. pseudo-Ag/AgCl) in a 0.10 mol L^{-1} PBS solution containing saturated dissolved O_2. (b) Capacitance complex spectra for poly(azo-BBY)-AuNPs before and after modification with immunosensor components. (c) Schematic representation of each step of immunosensor fabrication: (1) poly(azo-BBY)-AuNP; (2) poly(azo-BBY)-AuNP-Glu; (3) poly(azo-BBY)-AuNP-Glu-Ab; and (4) poly(azo-BBY)-AuNP-Glu-Ab-BSA.

Table 1
Impedimetric parameters determined by fitting the electrochemical impedance spectra of the immunosensor construction steps to the equivalent circuit shown in Fig. 1h. The errors presented for the fit were below 2%.

Modification step (Fig. 2c)	R_{Ω} (kΩ cm^2)	R_{ct}	R_{redox}	CPE_{dl} (µF cm^{-2} $s^{\alpha-1}$)	α_{dl}	CPE_{film} (µF cm^{-2} $s^{\alpha-1}$)	α_{film}	C_{redox} (µF cm^{-2})
(1)	0.10	0.483	22.4	4.10	0.96	26.2	0.60	5.40
(2)	0.10	0.565	55.8	6.93	0.95	18.4	0.65	6.12
(3)	0.10	0.211	36.1	9.06	0.96	11.2	0.61	7.79
(4)	0.10	0.276	112.0	2.90	0.80	7.39	0.82	3.68

containing dissolved O_2 saturated in atmospheric equilibrium. As shown in Fig. 3(a), there is an increase in the system impedance with the increase in concentration of 5-mC in solution as a function of the increase in surface blockage after binding between 5-mC and Ab-5-mC takes place. Therefore, a calibration curve was constructed (Fig. 3b and c) and shows a linear relationship between the relative R_{redox} and the logarithm of the 5-mC concentration (Eq. (3)). The proposed immunosensor reached a limit of detection (LOD) of 0.64 pg mL^{-1} and could be used for methylated DNA determination in unknown samples.

$$R_{relative}(\%) = 23.4 + 10.0log\left[5 - mC\left(ng\,mL^{-1}\right)\right] \quad \left(n = 5; r^2 = 0.9960\right) \tag{3}$$

4. Discussion

The remarkable structure of the poly(azo-BBY) film allows effective anchorage of biomolecules via free amine groups without affecting the structure of the azo group, which is responsible for the redox behavior of the polymer and the reduction reaction of dissolved oxygen molecules [15,16]. The presence of nanoparticles electrochemically synthesized in a single step in the same place made it possible to increase the sensitivity of the polymer toward dissolved oxygen molecules due to a significant increase in the active area surface [17,29]. This high sensitivity allowed monitoring of each step of immunosensor modification. It is clear that at each modification step, there was an increase in the number of species occupying and blocking the electrode surface, resulting in an increase in R_{redox} as a function of the "gate effect" generated for dissolved oxygen molecules to access the redox sites of the polymer [30,31]. Finally, the immunosensor was calibrated against different concentrations of 5-methylcytosine to explore the dissolved O_2 detection strategy. The promising response of the immuno-poly(azo-BBY)-AuNP-5mC immunosensor was compared with similar studies for the determination of

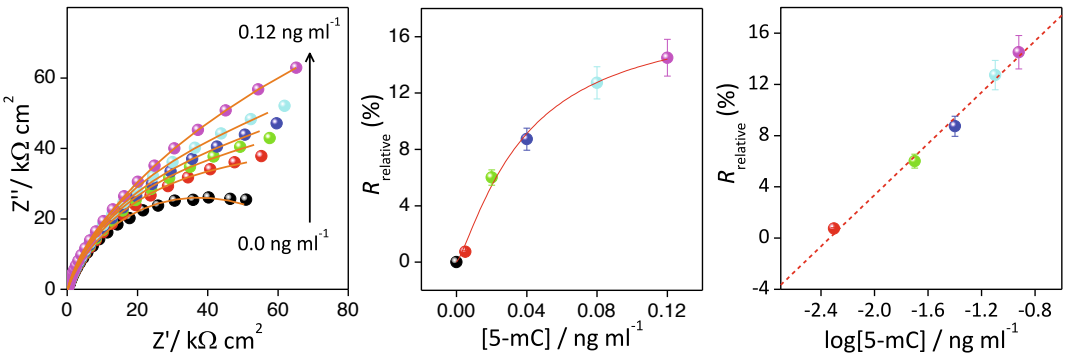

Fig. 3. Immunosensor evaluation. (a) Impedance spectra of the methylated DNA immunosensor with different concentrations of 5-mC in a solution of 0.05 mol L^{-1} PBS (pH 7.4), containing dissolved oxygen saturated in atmospheric equilibrium, with its calibration curves (b) and (c). The error bars represent the standard deviation obtained from three separate experiments using the same sensor.

methylated DNA, proving equivalent/superior to recent studies when comparing detection limits and quantification.

5. Conclusions

The new approach for building immunosensors based on the use of dissolved oxygen as a redox probe presented in this work is promising. Using the electropolymerization technique, the nanocomposite material was synthesized in a single step, saving time and reagents. Compared to conventional immunoassays based on electrochemical methods, a significant simplification of the sensory interface was achieved, which does not require an external redox probe, such as ferrocyanide, nor was it necessary to use markers or secondary antibodies for the analysis, simplifying the interface and decreasing the costs associated with the test.

CRediT authorship contribution statement

André Olean-Oliveira: Investigation, Visualization, Writing – original draft. **Patricia Monteiro Seraphim:** Visualization, Funding acquisition. **Marcos F.S. Teixeira:** Conceptualization, Methodology, Validation, Writing – review & editing, Supervision, Project administration, Funding acquisition.

Declaration of Competing Interest

The authors declare that they have no known competing financial interests or personal relationships that could have appeared to influence the work reported in this paper.

Acknowledgments

The authors acknowledge CEPID-FAPESP (2013/07296-2) and CNPq (303282/2020-7) for their financial support. A.O.O. thanks CAPES (88882.434480/2019-01) for the PhD fellowship. SJT.

Appendix A. Supplementary data

Supplementary data to this article can be found online at https://doi.org/10.1016/j.elecom.2022.107242.

References

[1] H. Karimi-Maleh, Y. Orooji, F. Karimi, M. Alizadeh, M. Baghayeri, J. Rouhi, S. Tajik, H.D. Beitollahi, S. Agarwal, V.K. Gupta, S. Rajendran, A. Ayati, L. Fu, A. L. Sanati, B. Tanhaei, F. Sen, M. Shabani-Nooshabadi, P.N. Asrami, A. Al-Othman, A critical review on the use of potentiometric based biosensors for biomarkers detection, Biosens. Bioelectron. 184 (2021), 113252, https://doi.org/10.1016/j.bios.2021.113252.

[2] A. Qureshi, J.H. Niazi, Biosensors for detecting viral and bacterial infections using host biomarkers: a review, Analyst 145 (24) (2020) 7825–7848, https://doi.org/10.1039/D0AN00896F.

[3] B.Y. Shao, Z.D. Xiao, Recent achievements in exosomal biomarkers detection by nanomaterials-based optical biosensors – A review, Anal. Chim. Acta 1114 (2020) 74–84, https://doi.org/10.1016/j.aca.2020.02.041.

[4] A. Khanmohammadi, A. Aghaie, E. Vahedi, A. Qazvini, M. Ghanei, A. Afkhami, A. Hajian, H. Bagheri, Electrochemical biosensors for the detection of lung cancer biomarkers: a review, Talanta 206 (2020) 120251, https://doi.org/10.1016/j.talanta.2019.120251.

[5] A. Yang, F. Yan, Flexible electrochemical biosensors for health monitoring, ACS Appl. Electron. Mater. 3 (1) (2021) 53–67, https://doi.org/10.1021/acsaelm.0c00534.

[6] S.S. Mahshid, S.E. Flynn, S. Mahshid, The potential application of electrochemical biosensors in the COVID-19 pandemic: a perspective on the rapid diagnostics of SARS-CoV-2, Biosens. Bioelectron. 176 (2021), 112905, https://doi.org/10.1016/j.bios.2020.112905.

[7] S. Menon, M.R. Mathew, S. Sam, K. Keerthi, K.G. Kumar, Recent advances and challenges in electrochemical biosensors for emerging and re-emerging infectious diseases, J. Electroanal. Chem. 878 (2020), 114596, https://doi.org/10.1016/j.jelechem.2020.114596.

[8] M. Urso, S. Tumino, E. Bruno, S. Bordonaro, D. Marletta, G.R. Loria, A. Avni, Y. Shacham-Diamand, F. Priolo, S. Mirabella, Ultrasensitive electrochemical impedance detection of Mycoplasma agalactiae DNA by low-cost and disposable Au-decorated NiO nanowall electrodes, ACS Appl. Mater. Inter. 12 (44) (2020) 50143–50151, https://doi.org/10.1021/acsami.0c14679.s001.

[9] A.D. Chowdhury, K. Takemura, T.C. Li, T. Suzuki, E.Y. Park, Electrical pulse-induced electrochemical biosensor for hepatitis E virus detection, Nat. Commun. 10 (2019) 3737, https://doi.org/10.1038/s41467-019-11644-5.

[10] T. Yang, S. Wang, H.L. Jin, W.W. Bao, S.M. Huang, J.C. Wang, An electrochemical impedance sensor for the label-free ultrasensitive detection of interleukin-6 antigen, Sensor. Actuat. B Chem. 178 (2013) 310–315, https://doi.org/10.1016/j.snb.2012.12.107.

[11] Y.H. Cheng, R. Kargupta, D. Ghoshal, Z.L. Li, C. Chande, L.X. Feng, S. Chatterjee, N. Koratkar, R.K. Motkuri, S. Basuray, ESSENCE-A rapid, shear-enhanced, flow-through, capacitive electrochemical platform for rapid detection of biomolecules, Biosens. Bioelectron. 182 (2021), 113163, https://doi.org/10.1016/j.bios.2021.113163.

[12] A. Baradoke, R. Hein, X. Li, J.J. Davis, Reagentless redox capacitive assaying of C-reactive protein at a polyaniline interface, Anal. Chem. 92 (5) (2020) 3508–3511, https://doi.org/10.1021/acs.analchem.9b0563310.1021/acs.analchem.9b05633.s001.

[13] A. Olean-Oliveira, G.A.O. Brito, C.X. Cardoso, M.F.S. Teixeira, Nanocomposite materials based on electrochemically synthesized graphene polymers: molecular architecture strategies for sensor applications, Chemosensors 9 (2021) 149, https://doi.org/10.3390/chemosensors9060149.

[14] A. Olean-Oliveira, T. Olean-Oliveira, A.C.R. Moreno, P.M. Seraphim, M.F. S. Teixeira, A chemiresistor sensor based on azo-polymer and graphene for real-time monitoring of mitochondrial oxygen consumption, ACS Sens. 4 (1) (2019) 118–125, https://doi.org/10.1021/acssensors.8b01013.

[15] A. Olean-Oliveira, M.F.S. Teixeira, Development of a nanocomposite chemiresistor sensor based on pi-conjugated azo polymer and graphene blend for detection of dissolved oxygen, Sensor. Actuat. B Chem 271 (2018) 353–357, https://doi.org/10.1016/j.snb.2018.05.128.

[16] M.F.S. Teixeira, M.M. Barsan, C.M.A. Brett, Molecular engineering of a pi-conjugated polymer film of the azo dye Bismarck Brown Y, RSC Adv. 6 (2016) 101318–101322, https://doi.org/10.1039/c6ra20335c.

[17] J. Han, M.G. Wang, Y.M. Hu, C.Q. Zhou, R. Guo, Conducting polymer-noble metal nanoparticle hybrids: synthesis mechanism application, Prog. Polym. Sci. 70 (2017) 52–91, https://doi.org/10.1016/j.progpolymsci.2017.04.002.

[18] A. Olean-Oliveira, G.A.O. Brito, M.F.S. Teixeira, Mechanism of nanocomposite formation in the layer-by-layer single-step electropolymerization of pi-conjugated azopolymers and reduced graphene oxide: an electrochemical impedance

spectroscopy study, ACS Omega 5 (2020) 25954–25967, https://doi.org/10.1021/acsomega.0c03391.
[19] P.V. Dudin, P.R. Unwin, J.V. Macpherson, Electrochemical nucleation and growth of gold nanoparticles on single-walled carbon nanotubes: new mechanistic insights, J. Phys. Chem. C 114 (31) (2010) 13241–13248, https://doi.org/10.1021/jp1043706.
[20] Y.A. Oliveira, A. Olean-Oliveira, M.F.S. Teixeira, Short communication: molecular architecture based on palladium-salen complex/graphene for low potential water oxidation, J. Electroanal. Chem. 880 (2021), 114928, https://doi.org/10.1016/j.jelechem.2020.114928.
[21] H.F. Trevizan, A. Olean-Oliveira, C.X. Cardoso, M.F.S. Teixeira, Development of a molecularly imprinted polymer for uric acid sensing based on a conductive azopolymer: unusual approaches using electrochemical impedance/capacitance spectroscopy without a soluble redox probe, Sensor. Actuat. B Chem. 343 (2021), 130141, https://doi.org/10.1016/j.snb.2021.130141.
[22] D.R. Walt, V.I. Agayn, The chemistry of enzyme and protein immobilization with glutaraldehyde, Trac-Trend Anal. Chem. 13 (10) (1994) 425–430, https://doi.org/10.1016/0165-9936(94)85023-2.
[23] Y. Xiao, S.N. Isaacs, Enzyme-linked immunosorbent assay (ELISA) and blocking with bovine serum albumin (BSA)–not all BSAs are alike, J. Immunol. Methods 384 (1-2) (2012) 148–151, https://doi.org/10.1016/j.jim.2012.06.009.
[24] R.Y. Wang, X.H. Zhou, X. Zhu, C. Yang, L.H. Liu, H.C. Shi, Isoelectric bovine serum albumin: robust blocking agent for enhanced performance in optical-fiber based DNA sensing, ACS Sens. 2 (2017) 257–262, https://doi.org/10.1021/acssensors.6b00746.
[25] S. Kurdyukov, M. Bullock, DNA methylation analysis: choosing the right method, Biology (Basel) 5 (2016), https://doi.org/10.3390/biology5010003.
[26] Z. Taleat, K. Mathwig, E.J.R. Sudholter, L. Rassaei, Detection strategies for methylated and hypermethylated DNA, Trac-Trend Anal. Chem. 66 (2015) 80–89, https://doi.org/10.1016/j.trac.2014.11.013.
[27] M.N. Islam, S. Yadav, M.H. Hague, A. Munaz, F. Islam, M.S. Al Hossain, V. Gopalan, A.K. Lam, N.T. Nguyen, M.J.A. Shiddiky, Optical biosensing strategies for DNA methylation analysis, Biosens. Bioelectron. 92 (2017) 668–678, https://doi.org/10.1016/j.bios.2016.10.034.
[28] O. Rapado-Gonzalez, C. Martinez-Reglero, A. Salgado-Barreira, M.A. Santos, R. Lopez-Lopez, A. Diaz-Lagares, M.M. Suarez-Cunqueiro, Salivary DNA methylation as an epigenetic biomarker for head and neck cancer. Part II: a cancer risk meta-analysis, J. Pers. Med. 11 (2021) 606, https://doi.org/10.3390/jpm11070606.
[29] S. Mahalakshmi, V. Sridevi, In situ electrodeposited gold nanoparticles on polyaniline-modified electrode surface for the detection of dopamine in presence of ascorbic acid and uric acid, Electrocatal. US 12 (2021) 415–435, https://doi.org/10.1007/s12678-021-00665-8.
[30] P. Lach, M. Cieplak, M. Majewska, K.R. Noworyta, P.S. Sharma, W. Kutner, “Gate effect” in p-synephrine electrochemical sensing with a molecularly imprinted polymer and redox probes, Anal. Chem. 91 (12) (2019) 7546–7553, https://doi.org/10.1021/acs.analchem.8b05512.
[31] J.P. Li, M. Sun, X.P. Wei, L.P. Zhang, Y. Zhang, An electrochemical aptamer biosensor based on “gate-controlled” effect using beta-cyclodextrin for ultra-sensitive detection of trace mercury, Biosens. Bioelectron. 74 (2015) 423–426, https://doi.org/10.1016/j.bios.2015.06.061.